Solar pilot plant scale hydrogen generation by irradiation of Cu/TiO$_2$ composites in presence of sacrificial electron donors

M.I. Maldonado[a,e,*], A. López-Martín[b], G. Colón[b], J. Peral[c,**], J.I. Martínez-Costa[d], S. Malato[a,e]

[a] *Plataforma Solar de Almería (CIEMAT), Carretera de Senés, km. 4, Tabernas, Almería, 04200, Spain*
[b] *Instituto de Ciencia de Materiales de Sevilla, Centro Mixto Universidad de Sevilla-CSIC, Américo Vespucio, 49, 41092, Sevilla, Spain*
[c] *Departament de Química, Universitat Autònoma de Barcelona, Edifici Cn, Bellaterra, Cerdanyola del Vallés, 08193, Spain*
[d] *Universidad Autónoma San Luis Potosí, Álvaro Obregón 64, C.P. 78000, San Luis Potosí, S.L.P., Mexico*
[e] *CIESOL, Centro de Investigación en Energía Solar, Centro Mixto Universidad de Almería-CIEMAT, 04120, Almería, Spain*

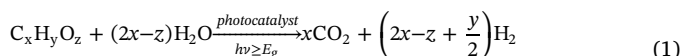## A R T I C L E   I N F O

A B S T R A C T

A Cu/TiO$_2$ photocatalyst has been synthesised by reducing a Cu precursor with NaBH$_4$ onto the surface of a sulphate pretreated TiO$_2$ obtained by a sol-gel procedure. The catalyst, that shows a clearly defined anatase phase with high crystallinity and relatively high surface area, and contains Cu$_2$O and CuO deposits on its surface, has been used to produce hydrogen in a solar driven pilot plant scale photocatalytic reactor. Different electron donor aqueous solutions (methanol, glycerol, and a real municipal wastewater treatment plant influent) have been tested showing similar or even higher energy efficiency than those obtained using more expensive noble metal based photocatalytic systems. The glycerol solutions have provided the best reactive environments for hydrogen generation.

1. Introduction

The ever-growing amount of energy consumed by mankind (currently based on fossil fuels) is causing unprecedented damage to our environment and, accordingly, the substitution of conventional energy sources by renewable-based ones is imperative. One of the most promising renewable alternatives involves the use of hydrogen as a fuel, since hydrogen can be produced from renewable resources and can be safely stored [1,2]. Hydrogen is considered an ideal energy carrier as it can store 3 times as much energy as conventional natural gas and its combustion is environmentally friendly [3]. Although the main current way of H$_2$ production involves the use of fossil fuels (steam reforming of methane), many efforts are underway to find new and reliable procedures for hydrogen generation using renewable energies [4]. In particular, since Fujishima and Honda [5] reported the photoelectrochemical hydrogen production back in 1972, many papers dealing with the generation of this gas from water by using semiconductor photocatalysts and light have been published [6–9]. As it has been repeatedly shown, the efficiency of the direct water splitting by heterogeneous photocatalysis is rather low, but hydrogen generation can be notably increased in presence of aqueous sacrificial agents (electron donors) [10–13]. Interestingly, aqueous pollutants can play the role of sacrificial agent and, consequently, simultaneous hydrogen production

and pollutant removal can take place, accordingly to the following global chemical Reaction (1):

$$C_xH_yO_z + (2x-z)H_2O \xrightarrow[h\nu \geq E_g]{photocatalyst} xCO_2 + \left(2x-z+\frac{y}{2}\right)H_2 \tag{1}$$

Titanium dioxide (TiO$_2$) has been widely tested in this reaction due to its high chemical stability, non-toxic character, strong oxidizing power and low price [14–18]. However, TiO$_2$ has a rather large band gap and that leaves visible light useless for photocatalyst activation. On the other hand, TiO$_2$ shows a large electron-hole recombination rate, something that limits the efficiency of the material as catalyst. Since noble metal nanoparticles (Pt or Au) can efficiently act as conduction band electrons traps [19] their deposition on the TiO$_2$ surface has helped to reduce the recombination rates and to remarkably increase reaction efficiencies. Nevertheless, the use of noble metals dramatically increases the cost of the photocatalyst rendering a useless material from a practical point of view. For that reason, cheaper metal deposits that could efficiently play the role of electron traps at a reasonable price are now investigated, being Cu one of the most promising candidates [20]. Because of the reactivity and the chemical versatility of Cu the deposition of nanoparticles of that metal onto the TiO$_2$ surface is not only interesting because of the production of a Cu° phase that plays the role of electron trap, but also for the formation of active Cu$_2$O and CuO

phases [21,22]. In this sense, the nature of the active copper species (Cu_2O or CuO), and other external factors governing their photoactivity is still not completely understood and many papers have tried to clarify this point [23,24]. Even the presence of other metal would critically affect the role and behavior of metal co-catalyst along the reaction [25].

Summarising, from the extensive results in the literature it can be pointed out that the capabilities of the incorporated copper species are: 1) to effectively separate the electron-hole pairs, thus reducing the occurrence of the recombination reaction, and 2) extend the light absorption to the visible range of the solar spectrum, especially with the incorporation of a Cu_2O phase, a semiconductor with a 2.0 eV bandgap and a conduction band edge position of 1.1 eV above the H^+/H_2 redox potential. However, it has to be considered that an extension of light absorption does not always clearly results into an enhancement of photocatalytic activity. Indeed, CuO has a bandgap of 1.4 eV that, in principle, should favour the absorption of visible light and improve the photocatalytic activity, but the conduction band edge position is slightly below the H^+/H_2 redox potential and thus its activity towards H_2 generation should be negligible. In reality, the work of several research groups has shown that the use of copper co-catalyst with other semiconductors, like TiO_2, renders important quantities of H_2, comparable in certain cases to noble metal candidates [14,26–30]. This fact clearly makes Cu-based photocatalysts an interesting candidate for large-scale production of H_2. In a recent paper, we have already shown that incorporation of Cu as co-catalyst by chemical reduction method would provide remarkable efficiencies for H_2 production [31]. In this work, we found that the optimal copper loading strongly depends on the preparation method, being for the present case around 3 mol%.

However, in addition to the catalyst optimization, the optimization of the process is crucial in order to make this attractive technology feasible under the industrial point of view. Some authors recently demonstrated that if technical progress is made to achieve an optimum photocatalyst and with appropriate plant-scale engineering, direct solar hydrogen produced from water by photoreforming can be produced at feasible costs below $2.90 per kilogram of hydrogen after compression and distribution, as suggested by the US Department of Energy [32,33]. Up to now, the low quantum efficiencies reported and the scarce scaling-up studies, lead to practical lack of industrial application for this attractive technology.

In this sense, a limited number of works about hydrogen generation via solar heterogeneous photocatalysis at pilot-plant scale have been reported so far [15,16,34–36]. Linkous et al. [37] carried out a series of experiments to guide development of reactor configurations for photochemical hydrogen production from H_2S solutions based on semiconductor particles. Platinized cadmium sulfide was utilized as the photocatalytic material, and powder suspensions, colloids, sedimentary dispersions and immobilized particle beds were studied at bench scale. Jing et al. [38] designed a Compound Parabolic Concentrator (CPC) for solar photocatalytic hydrogen production and they reported some preliminary results using CdS as photocatalyst but they failed to report the sacrificial agent used. Baniasadi et al. [36] analysed a photocatalytic energy conversion system for continuous production of hydrogen at a pilot-plant scale. The exergy efficiency, exergy destruction, environmental impact and sustainability index were investigated, and they also carried out exergonic environmental analyses. Finally, Villa et al. [15] and Arzate-Salgado et al. [16] presented pilot plant CPC experiments of photocatalytic hydrogen generation using N-doped TiO_2, CdS/ZnS and Au/TiO_2 catalysts in the same pilot plant used in the present work, and they showed that in all cases the system could work by using real wastewaters as source of sacrificial organic molecules.

The present study deals with a new reactive system and tries to bring more data to the shorty explored area of photocatalytic hydrogen generation under solar light irradiation and at large scale. The main objective is to evaluate the performance of a Cu/TiO_2 photocatalyst for the production of H_2 at a pilot-scale solar reactor by using different sacrificial electron donor species. The study also tries to assess the

Table 1
Main physicochemical characteristics of the demineralized water of PSA and municipal wastewater (MPTW) used in these experiments.

	Demineralized water	MPTW
Conductivity ($\mu S\, cm^{-1}$)	< 10	2000
DOC ($mg\, L^{-1}$)	< 0.5	100
Cl^- ($mg\, L^{-1}$)	0.7–0.8	425
SO_4^{2-} ($mg\, L^{-1}$)	0.5	123
pH	5-6	8.0

potential for hydrogen production with a real wastewater as source of electron donors. A special attention has been given to the influence of pH on the reaction efficiencies. A CPC reactor for photocatalytic water treatment has been used. This type of solar collector, designed with a concentration ratio of 1, is the best option to capture both the direct and diffuse radiation. Besides, it generally exhibits high optical and quantum efficiencies and low-cost [37,39].

2. Experimental

2.1. Reagents

All reagents used in this work were of analytical grade. High purity N_2 (99.9992%) was used to provide an O_2 free atmosphere. A commercial gas mixture of 1000 ppmv of H_2 in N_2 was used for GC calibration. Demineralised water from PSA (see Table 1 for main chemical composition) was used to prepare aqueous solutions. A municipal plant treated wastewater (MPTW), produced before the biological treatment in the Sewage Treatment Plant of Almería (Spain) was also used as source of electron donors. Table 1 also shows the main physicochemical characteristics of the municipal wastewater.

2.2. Catalysts preparation and characterisation

TiO_2 system was prepared by a sol-gel method using titanium tetraisopropoxide (TTIP) as precursor (10 mL TTIP) in water/isopropanol solution (200 mL iPrOH and 2 mL H_2O). Forced hydrolysis of the TTIP solution was achieved by adding certain volume of bidistilled water (8.4 mL). Finally the pH was adjusted to 9 by adding NH_4OH. The precipitate was then filtered, thoroughly washed with distilled water and dried at 120 °C overnight. The obtained TiO_2 precursor powder was then submitted to a sulfate pretreatment as reported in the literature [40]. Then, sulfation of TiO_2 precursor was performed by dispersing the fresh dried powders in a H_2SO_4 1 M solution (50 mL g^{-1}) for 1 h. Then, the suspension was filtered off and the powder dried again at 120 °C overnight. TiO_2 was finally obtained by calcination of sulfate treated powders at 650 °C for 2 h. As reported in previous papers, this pretreatment leads to a highly crystallized anatase TiO_2, preventing at the same time from surface sintering and providing exceptional surface and structural features [41,42]. The as-obtained sulfate pretreated TiO_2 was denoted as ST. Copper doping has been performed by chemical reduction by means of $NaBH_4$. Thus 1 g of ST was dispersed in 100 mL of water solution containing the corresponding stoichiometric amount of $Cu(NO_3)_2$ to achieve a metal loading of 2.5 wt%. Then an excess of $NaBH_4$ was added and the dispersion was thoroughly stirred for 1 h at room temperature. Finally this solution has been filtered, washed with distilled water and the obtained powder dried at 120 °C overnight. Thus obtained sample was labelled as CuST.

BET surface area measurements were carried out by N_2 adsorption at −196 °C using a Micromeritics 2000 instrument.

X-ray diffraction (XRD) patterns were obtained using a Siemens D-501 diffractometer with Ni filter and graphite monochromator. The X-ray source was Cu Kα radiation. From the line broadening of corresponding X-ray diffraction peaks, we have calculated the mean crystallite size according to Scherrer equation.

Diffuse reflectance spectra were obtained on a UV–vis scanning spectrophotometer Shimadzu AV2101, equipped with an integrating sphere, using BaSO$_4$ as reference. UV–vis spectra were performed in the diffuse reflectance mode (R) and transformed to a magnitude proportional to the extinction coefficient (K) through the Kubelka-Munk function, F(R$_\infty$). For the sake of comparison, all spectra were arbitrary normalized in intensity to 1. Band gap values were obtained from the plot of the modified Kubelka-Munk function (F(R$_\infty$)E)$^{1/2}$ versus the energy of the absorbed light E.

XPS data were recorded on $4 \times 4\,mm^2$ pellets, 0.5 mm thick, prepared by slightly pressing the powdered materials which were outgassed in the prechamber of the instrument at 105 °C up to a pressure $< 2 \times 10^{-8}$ torr to remove chemisorbed water from their surfaces. Spectra were recorded using a Leybold-Heraeus LHS-10 spectrometer, working with constant pass energy of 50 eV. The spectrometer main chamber, working at a pressure $< 2 \times 10^{-9}$ Torr, is equipped with an EA-200 MCD hemispherical electron analyser with a dual X-ray source working with Al Kα (hν = 1486.6 eV) at 120 W and 30 mA. C 1s signal (284.6 eV) was used as internal energy reference in all the experiments.

Transmission electron microscopy (TEM) and scanning electron microscopy (FE-SEM) were performed in a Philips CM200 and Hitachi S4800 microscopes respectively. The samples were dispersed in ethanol using an ultrasonicator and dropped on a carbon grid.

2.3. Photocatalytic runs

The pilot plant for photocatalytic hydrogen generation consisted of a closed stainless steel tank of 27 L of volume, fitted with gas and liquid inlet and outlet and a sampling port. Two parallel mass flow controllers could be used to control the desired N$_2$ gas flow into the reactor headspace during the reactor filling step. A centrifugal pump (PanWorld NH-100PX) with a flow rate of 20 L min^{-1} was used to recirculate the aqueous slurry from the tank to the tubes of the CPC. The photoreactor was composed of 16 Pyrex glass tubes (inner diameter 28.45 mm, outer diameter 32.0 mm, irradiated length 1401.0 mm) mounted on a fixed platform tilted 37° (local latitude). The total area and volume irradiated were 2.10 m^2 and 14.25 L, respectively. In all experiments, 25 L of solution were used (leaving 10.75 L in the dark distributed between the tank and the pumping pipelines, and a headspace in the tank of around 21.0 L). Different sacrificial agents were tested: glycerol, methanol (both at a 0.05 M concentration), and a municipal wastewater (see Table 1 for main chemical features).

At the beginning of each experiment the aqueous slurry was recirculated in the dark for 15 min to establish the adsorption–desorption equilibrium between organics and the photocatalyst and then the oxygen present in the gas phase volume was pulled out with pure N$_2$ until no more oxygen was detected. After that, the photoreactor was uncovered and the aqueous slurry was irradiated during 5 h. Gas samples were analysed at approximately 1 h intervals. The reactor headspace remained closed during the experiment (batch conditions).

When solar radiation is used as an energy source it is necessary to take into account its lack of steadiness and the fact that it changes during the same day or during different days (time of day, year season, meteorological conditions, etc.). Hence, in order to compare hydrogen generation data obtained in different experiments (or even at different times of the same experiment), it is necessary to normalize the data by using Eq. (2), where t$_n$ is the experimental time for each sample, W$_s$ the average solar radiation measured by the radiometer during the period Δt$_n$, V$_t$ is the total reactor volume, and A$_i$ is the irradiated area of the reactor (CPC). Q$_n$ (kJ L^{-1}) is the solar energy accumulated per reactor volume unit along the experiment, and it is used instead of the experimental time in order to take into account both experimental time and solar radiation evolution.

$$Q_n = Q_{n-1} + \Delta t_n\, W_s\, \frac{A_i}{V_t} \tag{2}$$

Solar radiation intensity was measured using a radiometer (KIPP& ZONNEN, CUV3 model) that provided data of the incident radiation corresponding to wavelengths below 400 nm (matching the absorption spectrum of TiO$_2$) and it was mounted on a platform at the same angle as the CPC. Data was recorded every minute in terms of W m^{-2}.

2.4. Analytical determinations

Hydrogen was analysed by using a gas micro-chromatograph (Agilent technologies 490) equipped with a TCD detector and a CP-MolSieve 5A column channel (10 m, with backflush and retention time stability). Pure N$_2$ was used as carrier gas. Organic degradation was quantified as dissolved organic carbon (DOC) by using a Shimadzu VCSH TOC analyser.

3. Results and discussions

From the structural point of view, the obtained sulfate preteated TiO$_2$ (ST support) shows well defined anatase phase in spite of the relatively high calcination temperature. As it has been previously reported, the sulfation pretreatment over amorphous TiO$_2$ precursor induces important structural and surface stabilization of anatase upon further calcination [40]. Thus, the calculated crystallite size (ca. 25 nm) and obtained surface area values (26 ± 2 m^2 g^{-1}) denote such structural and morphological stabilization upon calcination (Fig. 1a and c). This fact implies that the catalyst would show a high degree of crystallinity and a relatively high surface area value. As it is widely accepted, these factors are crucial in order to optimize the charge carrier diffusion after photoexcitation process.

Raman spectroscopy is often used for the structural characterization of materials, being in certain cases more sensitive than XRD to the appearance of residual phases. In the present case only Raman peaks corresponding to anatase TiO$_2$ can be detected (Fig. 1b). It has been extensively reported that anatase Eg peak located at ca. 150 cm^{-1}, associated to O−Ti−O symmetric stretching vibration, is very sensitive to the structural defects present [22]. The sharp profile of such peak clearly indicates the above stated high crystallinity of this catalyst. Since the incorporation of copper is only at the surface, as expected no effect on the structure is observed with respect to former ST (not shown).

As expected, CuST sample shows a great similarity in morphology to the parent ST reference. From SEM and TEM images it can be said that our material shows aggregated morphology formed by roundish small particles of ca. 26 nm (Fig. 2). This particle size is closely in accordance with the crystallite size obtained from XRD peak broadening (Fig. 1a). From EDS analysis (Fig. 2) it can be inferred that the distribution of copper on the particles is highly homogeneous indicating a good distribution of dopant on the TiO$_2$ surface.

From diffuse reflectance spectroscopy it is possible to discuss about the Cu species present at the surface (Fig. 3). Besides the TiO$_2$ absorption band it is possible to observe additional absorption contributions associated to CuO$_x$ species located in the visible range (400–800 nm) [43,44]. These new contributions can be clearly highlighted in the difference spectrum (inset in Fig. 3). It has been described that the band located at 210–270 nm is indicative of the O^{2-}(2p) → Cu^{2+}(3d) ligand-to-metal charge-transfer transition, where the Cu ions occupy isolated sites over the support. This band will appear overlapped by TiO$_2$ absorption band. Additionally, a band at 350 nm would indicate the formation of Cu^{1+} clusters (Cu−O−Cu)$^{2+}$ in a highly dispersed state [45]. A further band located at 400–500 nm might be assigned to the three-dimensional Cu^{1+} clusters in the CuO matrix due to a partial reduction of Cu^{2+} [46]. The d-d transition of the Cu^{2+} ion in the presence of the ligand (or crystal) field generated by ligand or oxygen ions has been reported to appear in the visible or near-infrared range. Finally, the absorption bands at 600–800 nm and 740–800 nm are assigned to 2E$_g$ → 2T$_{2g}$ transitions of Cu^{2+} located in the distorted
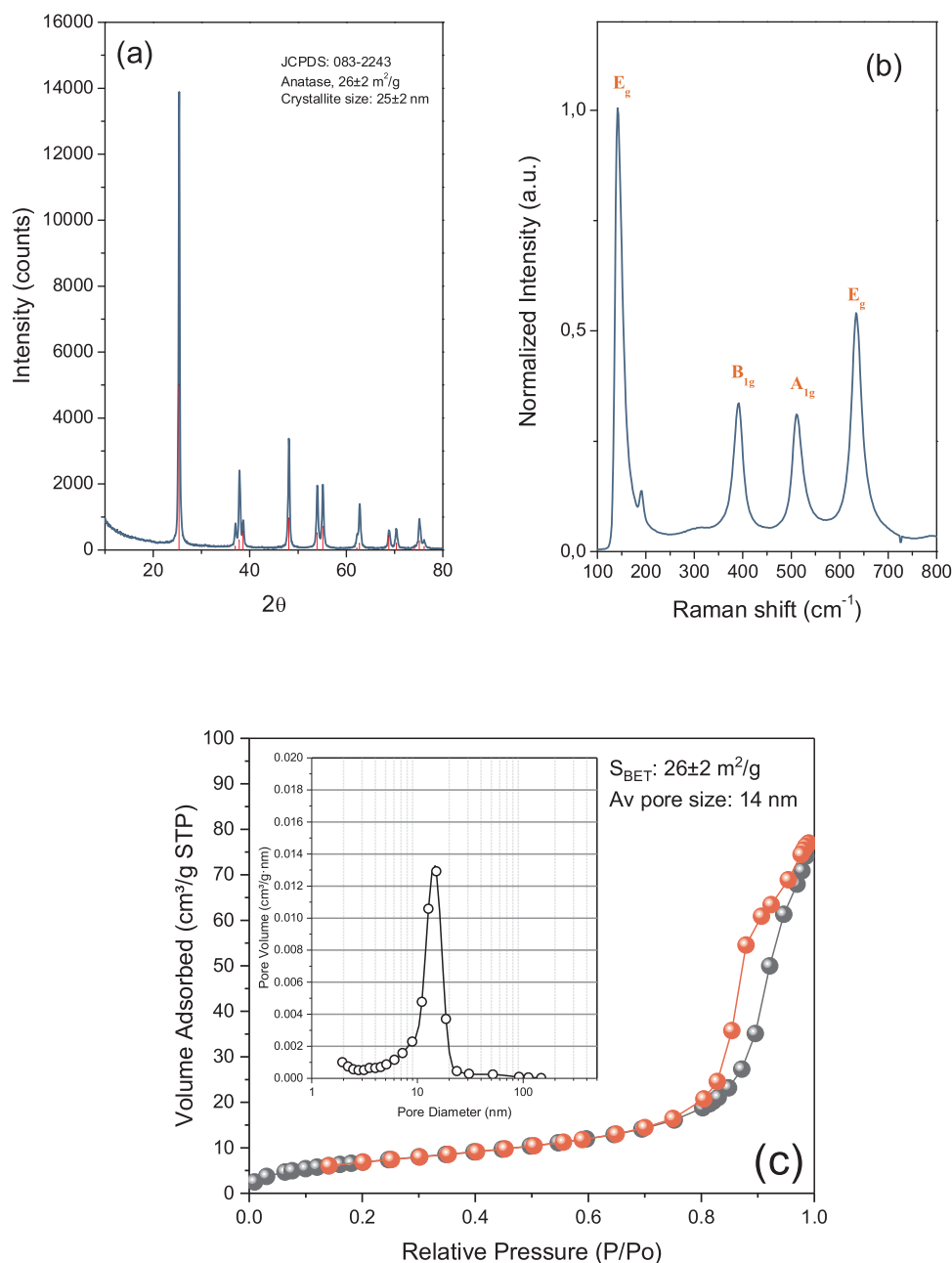
Fig. 1. Structural characterization of CuST photocatalyst: (a) X-ray diffraction pattern, (b) Raman spectrum and (c) N_2 adsorption-desorption isotherm and pore size distribution.

or perfect octahedral symmetry (Jahn–Teller effect), respectively [47].

Thus, from the difference spectrum, additional contributions at 420 and ca. 780 nm can be clearly noted. From these bands it can be stated that CuST sample new contributions at 440, 500 and 760 nm would point out the presence of both Cu^{1+} and Cu^{2+} [48].

The determination of the content as well as the nature and oxidation state of copper species has been accomplished using XPS technique. In Fig. 3 we show the Cu 2p spectra for the studied sample. Cu 2p curve is formed by two peaks located at ca. 932 and 934 eV which can be ascribed to Cu^{1+} and Cu^{2+}, respectively [49]. In addition, a shake-up satellite at ca. 943 eV also appears which is directly related to the Cu^{2+} species. From the curve deconvolution, it can be assessed that, Cu^{2+} is present in higher extent with respect to Cu^{1+}. Moreover, the chemical analysis of the sample denotes similar surface copper content and close to the nominal loadings (Cu/Ti = 0.3 vs. nominal 0.31). For these samples, Cu^{2+} arises as the predominant copper species at the surface. Thus, after chemical reduction, it can be evidenced that the final

powder suffers a reoxidation process probably during drying step.

The photocatalytic activity towards H_2 generation of the Cu/TiO_2 composite, prepared and characterized as described above, was tested under solar irradiation and at pilot plant scale by using different sacrificial electron donor species at different pH values. The tests started by using a simple organic probe molecule like methanol as sacrificial molecule. Methanol is especially suited to act as electron donor because of its lower splitting energy demand (16.1 KJ mol^{-1}) compared to water (237 KJ mol^{-1}) [50,51]. The choice of its initial concentration (0.05 M, DOC 600 mg L^{-1}) was aimed at simulate concentrations of organic compounds in real polluted waters. pHs values of 3, 9 and the natural pH of a 0.05 M methanol aqueous solution (6–7) were used. It has been noticed that pH values do not remain constant during the reactions. Small variations, always less than one pH unit, were observed. The same catalyst loading (0.2 g L^{-1} of Cu/TiO_2) was used through the entire study. This loading has been described as the optimum for the CPC photoreactor of outer diameter 32.0 mm [52] and
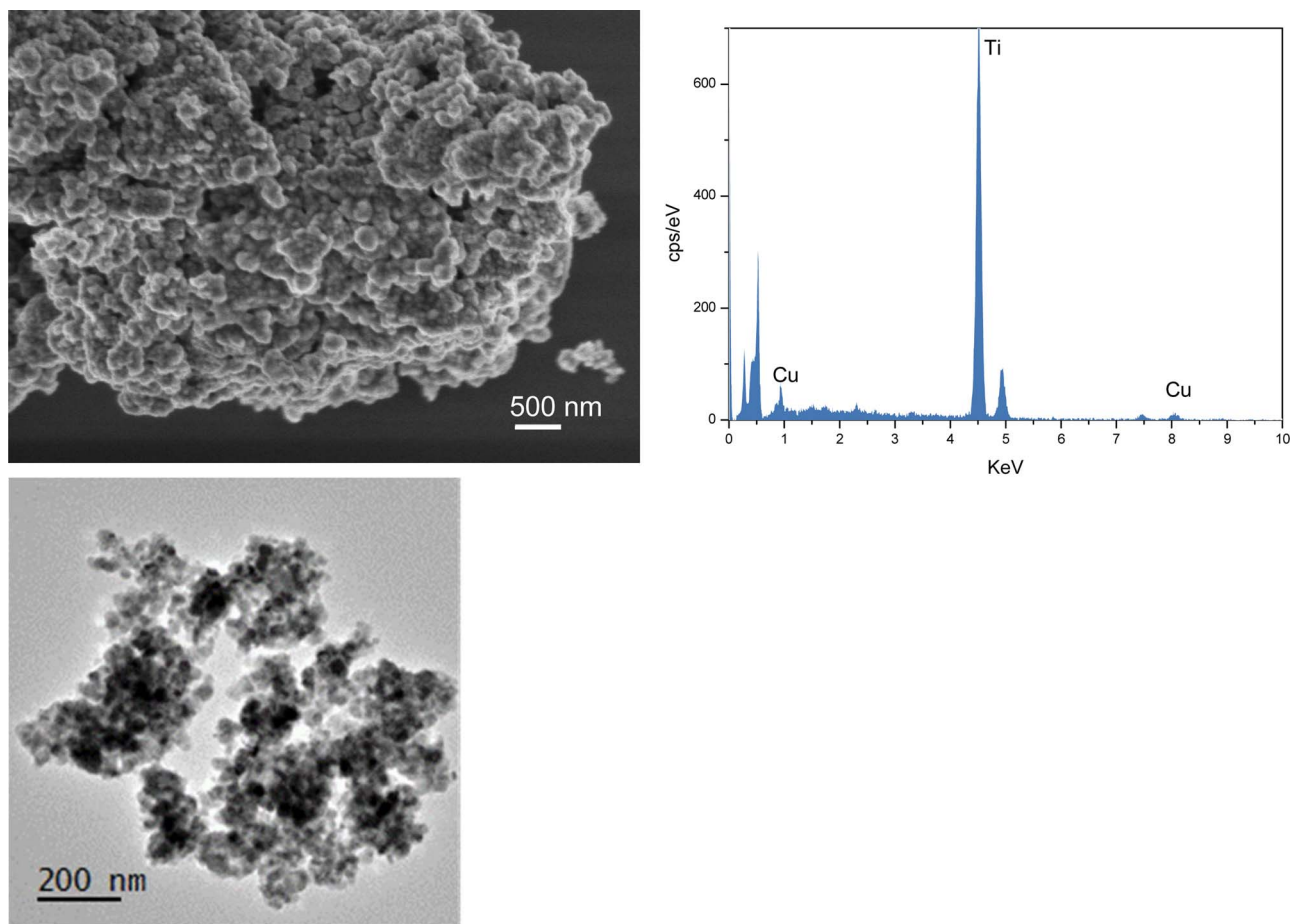
Fig. 2. SEM (with EDS analysis) and TEM images of CuST sample.

provided the best H$_2$ production in previous studies with other different catalytic systems at same operational conditions (the same location and reactor) [15,16]. Fig. 4 shows the H$_2$ evolution vs. the amount of energy accumulated into the reactor for those experiments with methanol. All experiments always lasted five hours although the final amount of energy accumulated into the reactor is different for each experiment, a consequence of the changes of solar radiation that take place along them. As can be seen, the neutral pH offers the best condition for H$_2$ production, while an acidic condition is clearly detrimental. At pH = 9 an intermediate behavior is noticed. This reactivity behavior in front of pH has been already observed by other authors when studying the photocatalytic generation of H$_2$ with Pt/TiO$_2$ catalysts [53]. Several

reasons could account for the improved rate of H$_2$ evolution at neutral and basic pH, including the effects of pH on (a) the positions of the valence and conduction band levels of the semiconductor with respect to those of the redox couples in solution, (b) the type of surface charge of the semiconductor, (c) the speciation of substances in solution, and (d) the size of photocatalyst particle aggregates formed. In any case, neutral-slightly basic pH offers the best condition for practical application as it is the usual pH in natural waters and many wastewaters.

A first and simple procedure that can be used to put in value the amounts of photogenerated H$_2$ is to compare the data generated in the present study with the H$_2$ generation by other photocatalytic systems previously studied using the same pilot plant reactor under similar
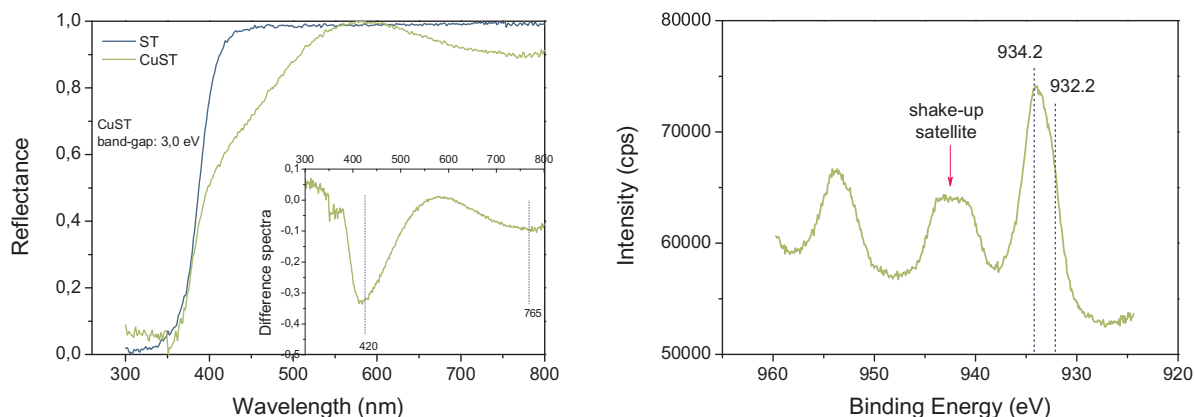

Fig. 3. DRS (inset: difference spectrum were obtained by subtracting CuST and ST spectra) and Cu2p XPS spectra of CuST.
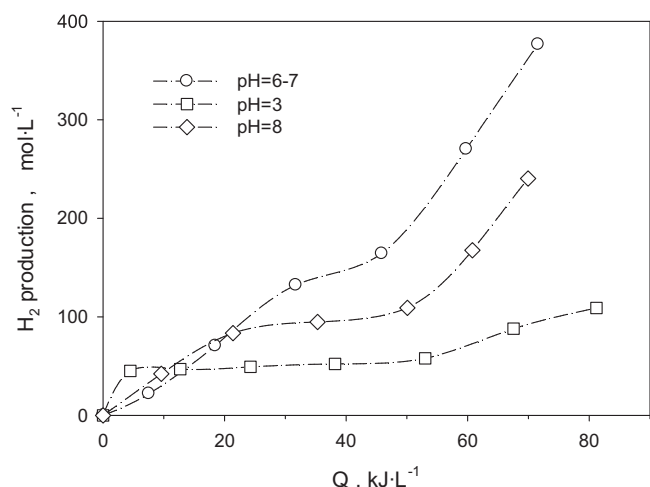
Fig. 4. Photocatalytic H_2 generation at different pH values by using methanol (0.05 M) as sacrificial electron donor. [Methanol] = 0.05 M and [Cu/TiO$_2$] = 0.2 g L^{-1}.
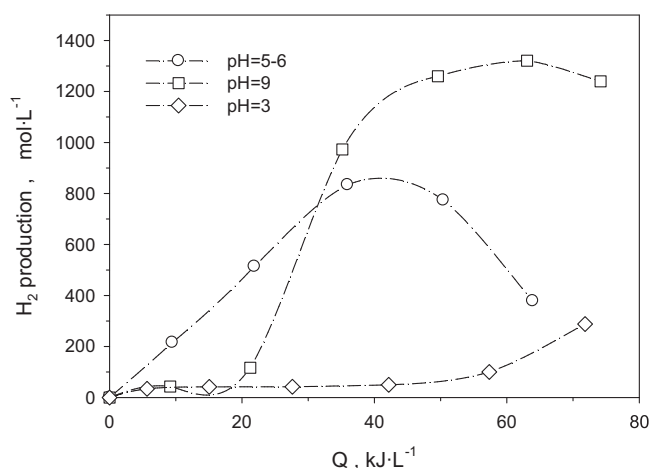

Fig. 5. Photocatalytic H_2 generation at different pH values by using glycerol (0.05 M) as sacrificial electron donor. [Glycerol] = 0.05 M and [Cu/TiO$_2$] = 0.2 g L^{-1}.

conditions. As seen in Fig. 4, a maximum production of H_2 of approximately 377 μmol L^{-1} at pH = 6–7 and after an energy accumulation of 71.6 kJ L^{-1} is detected (5.25 μmol kJ^{-1}), while the previous use of a Au/TiO$_2$ composite with methanol as electron donor, in the same reactor, with the same catalyst loading, produced 500 μmol L^{-1} after an energy accumulation around 100 kJ L^{-1} (5.0 μmol kJ^{-1}) [16]. Thus, at first sight the Cu/TiO$_2$ catalyst seems to be efficient, being able to produce a little bit more H_2 that the one generated with a Au/TiO$_2$ catalyst, although Au co-catalyst is prone to the capture the conduction band electrons and the elimination of electron-hole recombination, something that should, in principle, improve the hydrogen generation. This result is very interesting from an applied point of view since, as generally known, Cu is a much cheaper material than Au. As said above, the H_2 production with Cu/TiO$_2$ is still remarkable at other pH values, again probing this to be a rather simple photocatalytic system with a remarkable activity towards H_2 generation.

Simultaneously to the production of H_2 the dissolved organic carbon (DOC) content of the solution slightly decreased (16 mg L^{-1}), a decrease that provides more than the stoichiometric electrons needed for the observed H_2 generation. On the other hand, the temperature inside the reactor changed from around 15 °C at the beginning of the experiments (9:30–10:00 a.m.) to approximately 40 °C (normally around 1:00 p.m.) but no clear relation between the H_2 production rate and temperature has been noticed (data not shown).

Another set of experiments of photocatalytic hydrogen generation was carried out by using glycerol as sacrificial electron donor. It is well known that glycerol is produced and released in large quantities to the environment as by-product of the chemical reaction (transesterification) in which vegetable oils are processed into biodiesel [53]. Thus, glycerol is a good example of a waste product with attached disposal cost that could be used as feedstock for photocatalytic hydrogen production. Fig. 5 shows the H_2 evolution vs. the amount of energy accumulated into the reactor for those experiments with glycerol. As in the case of methanol, although the final energy accumulations for each experiment are different, they all belong to the same irradiation time (5 h). Again, the acidic pH conditions are the worse ones while the best initial H_2 production is obtained at pH close to neutral (5–6, the natural pH of the glycerol solution). However, for long irradiation times the production of H_2 at basic pH (around 9) is far better than at pH = 5–6. This fact could be explained by considering that glycerol photoreforming produces short chain organic acids which lower the pH in photocatalytic runs probably hampering the H_2 formation. Indeed, the experiment with glycerol at pH 5–6 shows a pH decay from 5.42 at the maximum hydrogen production (834 μmol L^{-1}) to 4.95 at the end of the run. In the case of pH 9, there is a pH variation throughout the

whole experiment from 9.41 to 6.36, i.e., the final pH is almost neutral and no deceleration of the hydrogen generation in the final half of the experiment it noticed.

Another remarkable fact is the large H_2 generation observed with glycerol. Indeed, the maximum amount of H_2 shown in Fig. 5 (at pH = 9) is 1240 μmol L^{-1}, 3.3 times larger than the best production with methanol at neutral pH, and in good agreement with previous works based on Cu-TiO$_2$ photocatalysis [54]. This is a quite remarkable result since, as pointed above, glycerol is an example of a real large scale waste molecule. As it will be discussed later, this H_2 generation lies among the best ones obtained with the same pilot plant reactor used in previous studies carried out by our group with other photocatalytic systems [15,16]. On the other hand the DOC removal detected in the glycerol solution was much more important (464 mg L^{-1} at pH = 9) than in the case of methanol (only a 16 mg L^{-1} removal at pH = 6–7), something in agreement with the much larger production of H_2.

A third group of photocatalytic experiments was carried out by using as sacrificial electron donors the organic compounds left in a real municipal wastewater before biological treatment. As seen in Table 1 that water contained around 100 mg L^{-1} of DOC but it was also a quite saline water with a high conductivity. The choice of this real wastewater, despite of the fact that its DOC content was clearly lower than the ones used in the experiments with methanol or glycerol synthetic solutions, was based on our previous experience about H_2 generation with other photocatalytic systems tested in the same reactor and with several real wastewater samples as sources of organic sacrificial molecules [16]. In those previous experiments the municipal wastewater was able to produce much more H_2 that an industrial wastewater with an initial DOC of 600 mg L^{-1}.

Fig. 6 shows the evolution of H_2 concentration in the headspace of the reactor vs. the solar energy accumulated at different pH values. Initially, very similar H_2 productions are attained for the three different pH tested, but after that initial period, and similarly to what has been seen in the previous case of water containing glycerol at neutral pH, the concentration of H_2 shows a clear decrease, probably due to the pH decrease that is produced by the oxidation of an high organic load and the generation of large amounts of organic acid by-products even at initial alkaline values of pH.

The removal of H_2 was more important in the reaction at pH = 3. The basic pH (pH = 10) produced a less important removal, while conditions close to neutral (pH = 7–8) left the maximum H_2 concentration. Since in this case the reaction responsible for the removal of H_2 is taking place at the three different pH tested it is reasonable to propose that the same side-reaction would occur during the methanol and glycerol photoreforming experiments. The fact that no decrease of total H_2 concentration is noticed for them (except for the case of
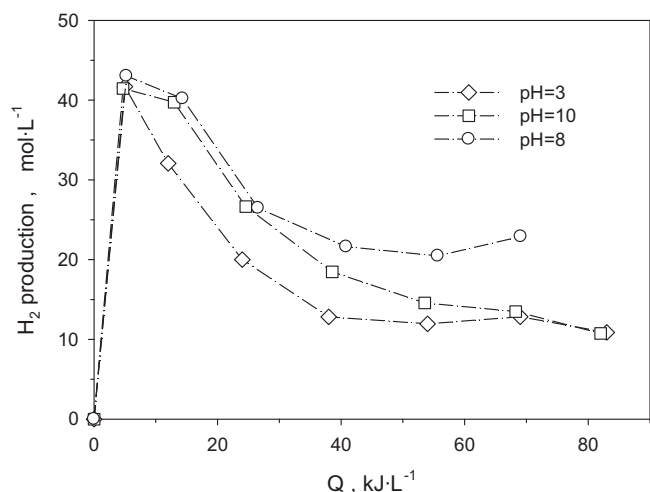
Fig. 6. Photocatalytic H_2 generation at different pH values by using a real municipal plant treated wastewater (see Table 1 for main chemical features) as sacrificial electron donor. $[Cu/TiO_2] = 0.2\,g\,L^{-1}$.

Fig. 8. H_2 production in consecutive photocatalytic experiments using the same sample of Cu/TiO_2 (recovered after each experiment and re-used in the following one). $[Methanol] = 0.05\,M$, $[Cu/TiO_2] = 0.2\,g\,L^{-1}$ and pH = 6–7.

glycerol at neutral pH) can be explained by considering photocatalytic H_2 generation rates that are equal of larger than H_2 consumption rates. In any case, when comparing the absolute values of H_2 production with the MPTW to those seen in Figs. 4 and 5 with methanol and glycerol it is clear that the real wastewater plays a poor role as reactive medium. Indeed, while a maximum production of $1240\,\mu mol\,L^{-1}$ of H_2 is attained with glycerol, only a maximum of $43\,\mu mol\,L^{-1}$ of H_2 are detected with the MPTW at pH = 7–8, i.e., a H_2 production that is almost 29 times lower. This poor performance detected when using a real wastewater was already reported for the photocatalytic production of H_2 with other reactive systems [15,16] and is most probably due to the high saline content of the samples that can passivate the photocatalyst surface or even compete for the capture of electrons and holes.

On the other hand, the temperature changed from 11 to 40 °C during the photocatalytic runs but, as in the previous cases with methanol and glycerol no clear relationship exists between temperature and H_2 production.

In the order to help the fast comparison of the H_2 productions with the different sacrificial agents and the different pH Fig. 7 displays the best H_2 generations of each experiment. As clearly seen the presence of glycerol at basic pH provides the best reaction conditions, while pH = 3
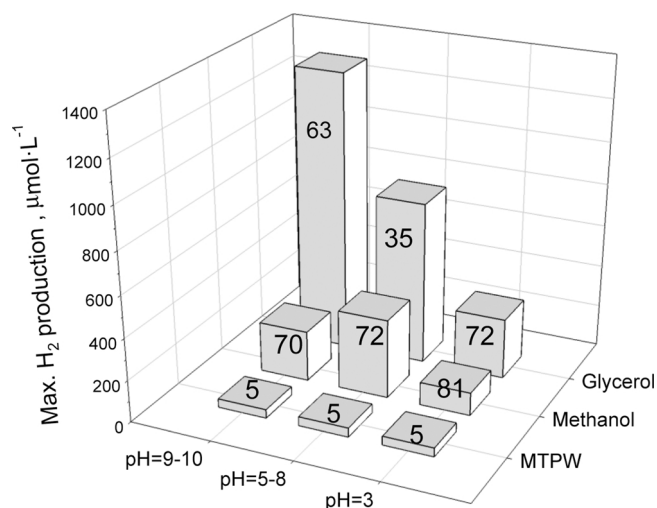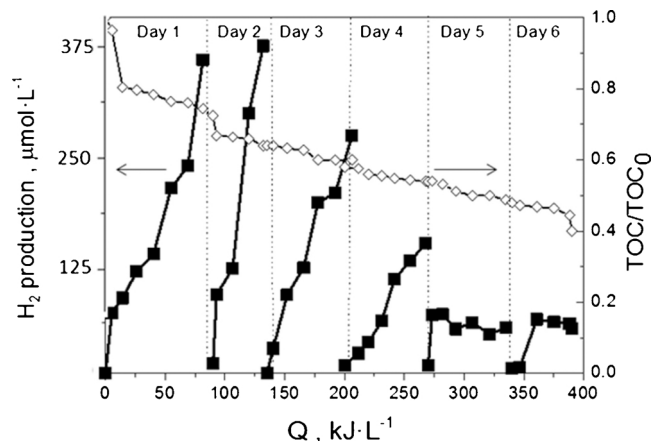
is detrimental for the three different samples, and the worst performances are always observed with the real wastewater samples. It is thus important to emphasize again over the outstanding large production of H_2 detected when using glycerol, something that makes the simple and cheap Cu/TiO_2 photocatalyst a potential candidate for real applications. On the other hand, and taking into account that after each of the experiments presented so far the amount of DOC remaining in solution was always high, consecutive experiments of H_2 production with the same reactive media (both the aqueous solutions and the photocatalyst powder) were carried out in an effort to check the long-term performance of this composite. Fig. 8 shows the consecutive H_2 production using an initial methanol 0.05 M aqueous solutions at pH = 6–7. As can be seen during the first and second runs the H_2 generation is quite similar (around $375\,\mu mol\,L^{-1}$) and no photocatalytic activity deactivation is noticed.

The DOC content after those two consecutive experiments is around 60% of the initial concentration. However, a clear decrease of activity is seen in the third experiment, with the maximum activity going down to $265\,\mu mol\,L^{-1}$, a decrease that is even worse in the following runs with final H_2 production activity (6th run) going all the way down to $56\,\mu mol\,L^{-1}$. This activity reduction should be expected because the organic content of the solution keeps decreasing with the consecutive runs ending up at a value of around 40% of the initial DOC. Thus, the reduction of the sacrificial electron donor concentration and the accumulation of by-products from methanol oxidation that, as formic acid, decrease the pH of the solution (the pH goes from 7.6 to 5.7 along the experiments), reduces the efficiency of the photocatalytic system (Fig. 8).

Finally, in an effort to have a more quantitative assessment of the capacity of this Cu/TiO_2 system to produce H_2, and to be able to carry out a more quantitative comparison with other photocatalytic systems the solar to hydrogen energy conversion (STH) of the reaction (amount of chemical energy stored in the produced H_2 vs. amount of solar energy accumulated in the CPC reactor) was calculated by using the following equation [55]:

$$\eta = \frac{\Delta G_{H_2}^0 \Delta H_2 V_g}{Q \cdot V_L} 100\% \tag{3}$$

where $\Delta G_{H_2}^0$ is the Gibbs free energy corresponding to the formed H_2 molecule ($283.6\,kJ\,mol^{-1}$), ΔH_2 is the total amount of hydrogen generated in a particular period of time (in $\mu mol\,L^{-1}$), Q is the useful solar energy accumulated in the CPC reactor during the same period of time (in $kJ\,L^{-1}$), considering the catalyst Eg ca 3.2 eV ($\lambda < 400\,nm$), and V_g and V_L are the volume of the gas and illuminated liquid phase of the reactor, respectively. In order to make those calculations we take into account the best hydrogen production rate reported, i.e.,

Fig. 7. Best H_2 productions for the different sacrificial electron donors and pH values tested $[Cu/TiO_2] = 0.2\,g\,L^{-1}$. The accumulated solar energy ($kJ\,L^{-1}$) associated to each energy production appears attached to each column.

856.2 μmol L^{-1} generated between minutes 120 and 180 during the experiment carried out with glycerol at pH = 9.

The solar energy accumulated into the reactor during those 60 min is 13.9 kJ L^{-1}. By using Eq. (3) a STH of 2.6% is obtained. Other more complex and expensive photocatalytic systems that were tested in the same pilot plant produced similar or less H$_2$: 2.5% and 1.6% STH for a Pt/(TiO$_2$-N) (a N doped TiO$_2$ with Pt deposits) and a Pt/(CdS-ZnS) photocatalysts, respectively [15], while a Au/TiO$_2$ photocatalyst, a much more expensive material with a more complex synthesis procedure gave only an slightly larger STH of 2.9% [16].

4. Conclusions

The search for the replacement of expensive solar driven photocatalysts for hydrogen production from water has shown that a simple an inexpensive Cu/TiO$_2$ photocatalyst can provide reaction yields that are similar to the ones obtained with materials like Au/TiO$_2$ or Pt/(TiO$_2$-N). The Cu/TiO$_2$ photocatalyst studied here has been simply synthesised by reducing a Cu precursor with NaBH$_4$ and with simultaneous deposition onto the surface of a sulphate pretreated TiO$_2$ obtained by a sol-gel procedure. From the structural characterization it is shown that the catalyst has a clearly defined anatase phase with high crystallinity and relatively high surface area (26 $\pm$ 2 m^2 g^{-1}). SEM and TEM images confirm that the new material is made of aggregates formed by roundish small particles of ca. 26 nm. Diffuse reflectance spectroscopy and XPS analysis indicate that the catalyst contains Cu$_2$O and CuO deposits on its surface. The photocatalytic hydrogen production has been carried out in a solar driven pilot plant scale photocatalytic reactor. Different electron donors like methanol, glycerol, and the organic content of a real municipal wastewater treatment plant effluent have been tested. The hydrogen productions at neutral or basic pH values have always been better that the ones at acid pH, and glycerol solutions have provided the best reactive environments for hydrogen generation. The outstanding performance for H$_2$ generation from glycerol appears as a markedly result considering the large quantities of this compound originated as waste material from the biodiesel production industry. The production of hydrogen with this inexpensive photocatalytic system is remarkable, leading to similar or even higher energy efficiency to those obtained by other more expensive photocatalytic systems.

Acknowledgments

References

[1] A. Kubacka, M. Fernández-García, G. Colón, Advanced nanoarchitectures for solar photocatalytic applications, Chem. Rev. 112 (2012) 1555–1614, http://dx.doi.org/10.1021/cr100454n.

[2] G. Zhang, X. Wan, A wind-hydrogen energy storage system model for massive wind energy curtailment, Int. J. Hydrogen Energy 39 (2014) 1243–1252, http://dx.doi.org/10.1016/j.ijhydene.2013.11.003.

[3] T.N. Vezirolu, F. Barbir, Hydrogen: the wonder fuel, Int. J. Hydrogen Energy 17 (1992) 391–404, http://dx.doi.org/10.1016/0360-3199(92)90183-W.

[4] O. Bičáková, P. Straka, Production of hydrogen from renewable resources and its effectiveness, Int. J. Hydrogen Energy 37 (2012) 11563–11578, http://dx.doi.org/10.1016/j.ijhydene.2012.05.047.

[5] A. Fujishima, K. Honda, Electrochemical photolysis of water at a semiconductor electrode, Nature 238 (1972) 37–38, http://dx.doi.org/10.1038/238037a0.

[6] A. Fujishima, X. Zhang, D.A. Tryk, Heterogeneous photocatalysis: from water photolysis to applications in environmental cleanup, Int. J. Hydrogen Energy 32 (2007) 2664–2672, http://dx.doi.org/10.1016/j.ijhydene.2006.09.009.

[7] S.W. Bae, S.M. Ji, S.J. Hong, J.W. Jang, J.S. Lee, Photocatalytic overall water splitting with dual-bed system under visible light irradiation, Int. J. Hydrogen Energy 34 (2009) 3243–3249, http://dx.doi.org/10.1016/j.ijhydene.2009.02.022.

[8] A. Kudo, Y. Miseki, Heterogeneous photocatalyst materials for water splitting,

[9] Chem. Soc. Rev. 38 (2009) 253–278, http://dx.doi.org/10.1039/B800489G.

[9] G. Colón, Towards the hydrogen production by photocatalysis, Appl. Catal. A: Gen. 518 (2016) 48–59, http://dx.doi.org/10.1016/j.apcata.2015.11.042.

[10] M.S. Park, M. Kang, The preparation of the anatase and rutile forms of Ag-TiO2 and hydrogen production from methanol/water decomposition, Mater. Lett. 62 (2008) 183–187, http://dx.doi.org/10.1016/j.matlet.2007.04.105.

[11] A. Patsoura, D.I. Kondarides, X.E. Verykios, Photocatalytic degradation of organic pollutants with simultaneous production of hydrogen, Catal. Today 124 (2007) 94–102, http://dx.doi.org/10.1016/j.cattod.2007.03.028.

[12] J. Wang, P. Yang, B. Cao, J. Zhao, Z. Zhu, Photocatalytic carbon-carbon bond formation with concurrent hydrogen evolution on the Pt/TiO2 nanotube, Appl. Surf. Sci. 325 (2015) 86–90, http://dx.doi.org/10.1016/j.apsusc.2014.10.143.

[13] Y. Xu, R. Xu, Nickel-based cocatalysts for photocatalytic hydrogen production, Appl. Surf. Sci. 351 (2015) 779–793, http://dx.doi.org/10.1016/j.apsusc.2015.05.171.

[14] S. Xu, A.J. Du, J. Liu, J. Ng, D.D. Sun, Highly efficient CuO incorporated TiO2 nanotube photocatalyst for hydrogen production from water, Int. J. Hydrogen Energy 36 (2011) 6560–6568, http://dx.doi.org/10.1016/j.ijhydene.2011.02.103.

[15] K. Villa, X. Domènech, S. Malato, M.I. Maldonado, J. Peral, Heterogeneous photocatalytic hydrogen generation in a solar pilot plant, Int. J. Hydrogen Energy (2013) 12718–12724, http://dx.doi.org/10.1016/j.ijhydene.2013.07.046.

[16] S.Y. Arzate Salgado, R.M. Ramírez Zamora, R. Zanella, J. Peral, S. Malato, M.I. Maldonado, Photocatalytic hydrogen production in a solar pilot plant using a Au/TiO2 photo catalyst, Int. J. Hydrogen Energy 41 (2016) 11933–11940, http://dx.doi.org/10.1016/j.ijhydene.2016.05.039.

[17] R. Dholam, N. Patel, M. Adami, A. Miotello, Physically and chemically synthesized TiO2 composite thin films for hydrogen production by photocatalytic water splitting, Int. J. Hydrogen Energy 33 (2008) 6896–6903, http://dx.doi.org/10.1016/j.ijhydene.2008.08.061.

[18] F. Xu, W. Xiao, B. Cheng, J. Yu, Direct Z-scheme anatase/rutile bi-phase nanocomposite TiO2 nanofiber photocatalyst with enhanced photocatalytic H2-production activity, Int. J. Hydrogen Energy 39 (2014) 15394–15402, http://dx.doi.org/10.1016/j.ijhydene.2014.07.166.

[19] S. Yang, H. Wang, H. Yu, S. Zhang, Y. Fang, S. Zhang, F. Peng, A facile fabrication of hierarchical Ag nanoparticles-decorated N-TiO2 with enhanced photocatalytic hydrogen production under solar light, Int. J. Hydrogen Energy 41 (2016) 3446–3455, http://dx.doi.org/10.1016/j.ijhydene.2015.12.190.

[20] L. Clarizia, D. Spasiano, I. Di Somma, R. Marotta, R. Andreozzi, D.D. Dionysiou, Copper modified-TiO2 catalysts for hydrogen generation through photoreforming of organics. A short review, Int. J. Hydrogen Energy 39 (2014) 16812–16831, http://dx.doi.org/10.1016/j.ijhydene.2014.08.037.

[21] L. Clarizia, G. Vitiello, D.K. Pallotti, B. Silvestri, M. Nadagouda, S. Lettieri, G. Luciani, R. Andreozzi, P. Maddalena, R. Marotta, Effect of surface properties of copper-modified commercial titanium dioxide photocatalysts on hydrogen production through photoreforming of alcohols, Int. J. Hydrogen Energy 42 (2017) 28349–28362, http://dx.doi.org/10.1016/j.ijhydene.2017.09.093.

[22] S. Obregón, A. Kubacka, M. Fernández-García, G. Colón, High-performance Er3 + -TiO2 system: dual up-conversion and electronic role of the lanthanide, J. Catal. 299 (2013) 298–306, http://dx.doi.org/10.1016/j.jcat.2012.12.021.

[23] Q. Hu, J. Huang, G. Li, Y. Jiang, H. Lan, W. Guo, Y. Cao, Origin of the improved photocatalytic activity of Cu incorporated TiO2 for hydrogen generation from water, Appl. Surf. Sci. 382 (2016) 170–177, http://dx.doi.org/10.1016/j.apsusc.2016.04.126.

[24] Z. He, J. Fu, B. Cheng, J. Yu, S. Cao, Cu2(OH)2CO3 clusters: novel noble-metal-free cocatalysts for efficient photocatalytic hydrogen production from water splitting, Appl. Catal. B: Environ. 205 (2017) 104–111, http://dx.doi.org/10.1016/j.apcatb.2016.12.031.

[25] M.J. Muñoz-Batista, D. Motta Meira, G. Colón, A. Kubacka, M. Fernández-García, Phase-contact engineering in mono and bimetallic Cu-Ni co-catalysts for hydrogen photo-production materials, Angew. Chem. Int. Ed. 57 (2018) 1199.

[26] S. Xu, D.D. Sun, Significant improvement of photocatalytic hydrogen generation rate over TiO2 with deposited CuO, Int. J. Hydrogen Energy 34 (2009) 6096–6104, http://dx.doi.org/10.1016/j.ijhydene.2009.05.119.

[27] J.M. Kum, S.H. Yoo, G. Ali, S.O. Cho, Photocatalytic hydrogen production over CuO and TiO2 nanoparticles mixture, Int. J. Hydrogen Energy 38 (2013) 13541–13546, http://dx.doi.org/10.1016/j.ijhydene.2013.08.004.

[28] W.T. Chen, V. Jovic, D. Sun-Waterhouse, H. Idriss, G.I.N. Waterhouse, The role of CuO in promoting photocatalytic hydrogen production over TiO2, Int. J. Hydrogen Energy 38 (2013) 15036–15048, http://dx.doi.org/10.1016/j.ijhydene.2013.09.101.

[29] Y.-H. Yu, Y.-P. Chen, Z. Cheng, Microwave-assisted synthesis of rod-like CuO/TiO2 for high-efficiency photocatalytic hydrogen evolution, Int. J. Hydrogen Energy 40 (2015) 15994–16000, http://dx.doi.org/10.1016/j.ijhydene.2015.09.115.

[30] Q. Hu, J. Huang, G. Li, J. Chen, Z. Zhang, Z. Deng, Y. Jiang, W. Guo, Y. Cao, Effective water splitting using CuOx/TiO2 composite films: role of Cu species and content in hydrogen generation, Appl. Surf. Sci. 369 (2016) 201–206, http://dx.doi.org/10.1016/j.apsusc.2016.01.281.

[31] J.M. Valero, S. Obrego, G. Colon, Active site considerations on the photocatalytic H2 evolution performance of Cu-doped TiO2 obtained by different doping methods, ACS Catal. 4 (2014) 3320–3329, http://dx.doi.org/10.1021/cs500865y.

[32] B.A. Pinaud, J.D. Benck, L.C. Seitz, A.J. Forman, Z. Chen, T.G. Deutsch, B.D. James, K.N. Baum, G.N. Baum, S. Ardo, H. Wang, E. Miller, T.F. Jaramillo, Technical and economic feasibility of centralized facilities for solar hydrogen production via photocatalysis and photoelectrochemistry, Energy Environ. Sci. 6 (2013) 1983, http://dx.doi.org/10.1039/c3ee40831k.

[33] C.A. Rodriguez, M.A. Modestino, D. Psaltis, C. Moser, Design and cost

considerations for practical solar-hydrogen generators, Energy Environ. Sci. 7 (2014) 3828–3835, http://dx.doi.org/10.1039/C4EE01453G.

[34] H. Cheng, K. Fuku, Y. Kuwahara, K. Mori, H. Yamashita, Harnessing single-active plasmonic nanostructures for enhanced photocatalysis under visible light, J. Mater. Chem. A 3 (2015) 5244–5258, http://dx.doi.org/10.1039/C4TA06484D.

[35] B. Gupta, A.A. Melvin, T. Matthews, S. Dash, A.K. Tyagi, TiO2 modification by gold (Au) for photocatalytic hydrogen (H2) production, Renew. Sustain. Energy Rev. 58 (2016) 1366–1375, http://dx.doi.org/10.1016/j.rser.2015.12.236.

[36] E. Baniasadi, I. Dincer, G.F. Naterer, Exergy and environmental impact assessment of solar photoreactors for catalytic hydrogen production, Chem. Eng. J. 213 (2012) 330–337, http://dx.doi.org/10.1016/j.cej.2012.10.018.

[37] C.A. Linkous, N.Z. Muradov, S.N. Ramser, Consideration of reactor design for solar hydrogen production from hydrogen sulfide using semiconductor particulates, Int. J. Hydrogen Energy 20 (1995) 701–709.

[38] D. Jing, H. Liu, X. Zhang, L. Zhao, L. Guo, Photocatalytic hydrogen production under direct solar light in a CPC based solar reactor: reactor design and preliminary results, Energy Convers. Manag. 50 (2009) 2919–2926, http://dx.doi.org/10.1016/j.enconman.2009.07.012.

[39] S. Malato, P. Fernández-Ibáñez, M.I. Maldonado, J. Blanco, W. Gernjak, Decontamination and disinfection of water by solar photocatalysis: recent overview and trends, Catal. Today 147 (2009) 1–59, http://dx.doi.org/10.1016/j.cattod.2009.06.018.

[40] G. Colón, M.C. Hidalgo, G. Munuera, I. Ferino, M.G. Cutrufello, J.A. Navío, Structural and surface approach to the enhanced photocatalytic activity of sulfated TiO2 photocatalyst, Appl. Catal. B: Environ. 63 (2006) 45–59, http://dx.doi.org/10.1016/j.apcatb.2005.09.008.

[41] M.C. Hidalgo, M. Maicu, J.A. Navío, G. Colón, Study of the synergic effect of sulphate pre-treatment and platinisation on the highly improved photocatalytic activity of TiO2, Appl. Catal. B: Environ. 81 (2008) 49–55, http://dx.doi.org/10.1016/j.apcatb.2007.11.036.

[42] M.C. Hidalgo, M. Maicu, J.A. Navío, G. Colón, Effect of sulfate pretreatment on gold-modified TiO2 for photocatalytic applications, J. Phys. Chem. C 113 (2009) 12840–12847, http://dx.doi.org/10.1021/jp903432p.

[43] B. Choudhury, A. Choudhury, Local structure modification and phase transformation of TiO2 nanoparticles initiated by oxygen defects, grain size, and annealing temperature, Int. Nano Lett. 3 (2013) 55, http://dx.doi.org/10.1186/2228-5326-3-55.

[44] B. Montanari, A. Vaccari, M. Gazzano, P. Kassner, H. Papp, J. Pasel, R. Dziembaj, W. Makowski, T. Lojewski, Characterization and activity of novel copper-containing catalysts for selective catalytic reduction of NO with NH3, Appl. Catal. B: Environ. 13 (1997) 205–217, http://dx.doi.org/10.1016/S0926-3373(96)00106-3.

[45] W. Lin, H. Frei, Photochemical CO2 splitting by metal-to-metal charge-transfer excitation in mesoporous ZrCu(l)-MCM-41 silicate sieve, J. Am. Chem. Soc. 127 (2005) 1610–1611, http://dx.doi.org/10.1021/ja040162l.

[46] M. Lenglet, K. Kartouni, D. Delahaye, Characterization of copper oxidation by linear potential sweep voltammetry and UV–vis-NIR diffuse reflectance spectroscopy, J. Appl. Electrochem. 21 (1991) 697–702, http://dx.doi.org/10.1007/BF01034048.

[47] M. Crivello, C. Pérez, E. Herrero, G. Ghione, S. Casuscelli, E. Rodríguez-Castellón, Characterization of Al-Cu and Al-Cu-Mg mixed oxides and their catalytic activity in dehydrogenation of 2-octanol, Catal. Today (2005) 215–222, http://dx.doi.org/10.1016/j.cattod.2005.07.168.

[48] S. Velu, K. Suzuki, M. Okazaki, M.P. Kapoor, T. Osaki, F. Ohashi, Oxidative steam reforming of methanol over CuZnAl(Zr)-oxide catalysts for the selective production of hydrogen for fuel cells: catalyst characterization and performance evaluation, J. Catal. 194 (2000) 373–384, http://dx.doi.org/10.1006/jcat.2000.2940.

[49] H. Zhu, M. Du, D. Yu, Y. Wang, L. Wang, M. Zou, M. Zhang, Y. Fu, A new strategy for the surface-free-energy-distribution induced selective growth and controlled formation of Cu2O–Au hierarchical heterostructures with a series of morphological evolutions, J. Mater. Chem. A 1 (2013) 919–929, http://dx.doi.org/10.1039/C2TA00591C.

[50] W.C. Lin, W.D. Yang, I.L. Huang, T.S. Wu, Z.J. Chung, Hydrogen production from methanol/water photocatalytic decomposition using pt/tio2-xnx catalyst, Energy Fuels 23 (2009) 2192–2196, http://dx.doi.org/10.1021/ef801091p.

[51] P. Chowdhury, G. Malekshoar, A. Ray, Dye-sensitized photocatalytic water splitting and sacrificial hydrogen generation: current status and future prospects, Inorganics 5 (2017) 34, http://dx.doi.org/10.3390/inorganics5020034.

[52] J. Colina-Márquez, F. MacHuca-Martínez, G.L. Puma, Radiation absorption and optimization of solar photocatalytic reactors for environmental applications, Environ. Sci. Technol. 44 (2010) 5112–5120, http://dx.doi.org/10.1021/es100130h.

[53] V.M. Daskalaki, D.I. Kondarides, Efficient production of hydrogen by photo-induced reforming of glycerol at ambient conditions, Catal. Today 144 (2009) 75–80, http://dx.doi.org/10.1016/j.cattod.2008.11.009.

[54] L. Clarizia, G. Vitiello, G. Luciani, I. Di Somma, R. Andreozzi, R. Marotta, In situ photodeposited nano Cu on TiO2 as a catalyst for hydrogen production under UV/vis radiation, Appl. Catal. A: Gen. 518 (2016) 142–149, http://dx.doi.org/10.1016/j.apcata.2015.07.044.

[55] Q. Wang, T. Hisatomi, Q. Jia, H. Tokudome, M. Zhong, C. Wang, Z. Pan, T. Takata, M. Nakabayashi, N. Shibata, Y. Li, I.D. Sharp, A. Kudo, T. Yamada, K. Domen, Scalable water splitting on particulate photocatalyst sheets with a solar-to-hydrogen energy conversion efficiency exceeding 1%, Nat. Mater. 15 (2016) 611–615, http://dx.doi.org/10.1038/nmat4589.